Title

Efficient Computation of the 2-D Green's Function for 1-D Periodic Structures Using the Ewald Method

Permalink

https://escholarship.org/uc/item/6vd3x1c2

Authors

Capolino, Filippo

Wilton, Donald R

Johnson, William A

Peer reviewed

Efficient Computation of the 2-D Green's Function for 1-D Periodic Structures Using the Ewald Method

Filippo Capolino, *Senior Member, IEEE*, Donald R. Wilton, *Fellow, IEEE*, and
William A. Johnson, *Senior Member, IEEE*

Abstract—The Ewald method is applied to accelerate the evaluation of the Green's function of an infinite periodic phased array of line sources. The Ewald representation for a cylindrical wave is obtained from the known representation for the spherical wave, and a systematic general procedure is applied to extend previous results. Only a few terms are needed to evaluate Ewald sums, which are cast in terms of error functions and exponential integrals, to high accuracy. Singularities and convergence rates are analyzed, and a recipe for selecting the Ewald splitting parameter $\mathcal{E}$ is given to handle both low and high frequency ranges. Indeed, it is shown analytically that the choice of the standard optimal splitting parameter $\mathcal{E}_0$ will cause overflow errors at high frequencies. Numerical examples illustrate the results and the sensitivity of the Ewald representation to the splitting parameter $\mathcal{E}$.

Index Terms—Arrays, series acceleration, fast methods, green function, gratings, numerical methods, periodic structures.

I. INTRODUCTION

IN APPLYING numerical full wave methods to periodic structures, fast and accurate means for evaluating the periodic Green's function are often needed. Among various techniques to accelerate computation of the Green's function is the Ewald method, originally developed by P. P. Ewald in [1], and extended to the case of the free space Green's function for three-dimensional (3-D) problems with two-dimensional (2-D) periodicity (i.e., a planar array of dipoles) in [2], and for 2-D problems in [3]. Its application in evaluating Green's functions for multilayered media is treated in [4] and [5], while its application in evaluating Green's functions for a rectangular cavity is reported in [6]. The Ewald method is extended in [3] to 2-D problems with one-dimensional (1-D) periodicity (i.e., a planar array of line sources) for the case of coplanar source and observation points. A brief summary on extending the approach to the noncoplanar case also appears in [3], in which a formula

for noncoplanar source and observation points was obtained by integrating in closed form the results in [2].

We present here an alternative direct procedure for applying the Ewald approach to obtain the Green's function for an array of line sources with 1-D periodicity. The approach is the 2-D analog of that of [2]. In this approach the Ewald representation for the basic cylindrical wavefunction (Hankel function) is obtained from that for the spherical wave given in [2]. While the paper was in print, we have found that a similar procedure was derived in [7], where performances of various Green's function representations for 2-D periodic arrays are compared.

As previously noted in [8], at high frequencies such that the wavelength is somewhat smaller than the period, computing the Ewald series using the optimal splitting parameter $\mathcal{E}_0$ (see [2]) may yield inaccurate results due to the finiteness of machine precision. In [8], it is suggested that such numerical inaccuracies may be improved by increasing the value of the splitting parameter $\mathcal{E}$ as frequency increases. Here, we present for the first time an algorithm for choosing the Ewald splitting parameter $\mathcal{E}$ that extends the efficiency of the method when the wavelength is somewhat larger or smaller than the periodicity. The proposed algorithm is efficiently applied to periodic structures when the observation point is near the planar array of sources. The critical distance from the array plane beyond which the Ewald method is not advantageous compared to the standard spectral grating lobe series is analyzed in [9].

II. STATEMENT OF THE PROBLEM

Consider the element-by-element superposition of the fields radiated by the infinite phased array of line sources

$$G(\mathbf{r}, \mathbf{r}') = \sum_{m=-\infty}^{\infty} e^{-jk_{x0}md} \frac{1}{4j} H_0^{(2)}(kR_m) \qquad (1)$$

where

$$k_{x0} = k\cos\theta_0 \qquad (2)$$

is the component of the phase gradient along the x direction with equivalent scan angle θ_0 and

$$R_m = \sqrt{(z-z')^2 + (x-x'-md)^2} \qquad (3)$$

is the distance between the observation point $\mathbf{r} \equiv (x, z)$ and the mth source point $\mathbf{r}'_m \equiv (x'+md, z')$ (see Fig. 1). Terms in the series (1) are of order $1/\sqrt{m}$ for large m, so that the series is extremely slowly convergent. An alternative plane wave series representation of this Green's function also exists, but it
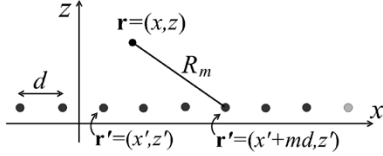
Fig. 1. Physical configuration and coordinates for a planar periodic array of line sources with interelement spacing d along x. $R_m = \sqrt{(x - x' - md)^2 + (z - z')^2}$ is the distance between observation point $\mathbf{r} \equiv (x, z)$ and the nth source element $\mathbf{r}' \equiv (x' + md, z')$.
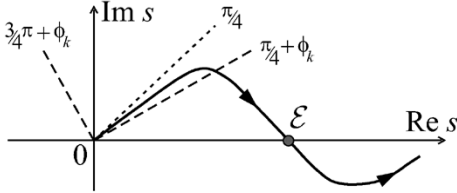

Fig. 2. Path of integration. Expressing $k = |k| \exp(j\phi_k)$ (Im $k \leq 0$, thus $\phi_k < 0$), and $s = |s| \exp(j\phi_s)$, the region of convergence of (8) is $(3/4)\pi + \phi_k \geq \phi_s \geq \pi/4 + \phi_k$ for $s \to 0$, and $\pi/4 > \phi_s > -\pi/4$ for $s \to \infty$.

is also slowly convergent. Here we transform (1) into a rapidly converging series.

III. EWALD TRANSFORMATION FOR 2-D PROBLEMS

For simplicity the homogeneous medium is assumed to have small losses and a complex ambient wavenumber $k = k_r + jk_i$, with $k_i < 0$. The Ewald transformation for the cylindrical (2-D) radiated field is obtained by integrating in y' both members of the Ewald transformation for the spherical (3-D) radiated field [2]

$$\frac{e^{-jk\sqrt{R^2+(y-y')^2}}}{4\pi\sqrt{R^2+(y-y')^2}} = \frac{1}{2\pi^{3/2}} \int_0^\infty e^{-[R^2+(y-y')^2]s^2+\frac{k^2}{4s^2}} ds$$

(4)

where the integration path in the complex plane is shown in Fig. 2. This contour differs from that of [2, p. 226, Fig. 1] because an $\exp(j\omega t)$ convention has been chosen here. The reasons for this particular choice for the shape of the integration path are explained in the following and specific constraints are given for the integrability of the integrand on that specific path. It is useful to write the ambient wavenumber in polar coordinates $k = |k|e^{j\phi_k}$, with $\phi_k = \arctan(k_i/k_r) < 0$, and $s = s_r + js_i = |s| \exp(j\phi_s)$ with $\phi_s = \arctan(s_i/s_r)$. Indeed, convergence of (4) is ensured by requiring that $\text{Re}[k^2/s^2] < 0$ for $s \to 0$, and $\text{Re} s^2 > 0$ for $s \to \infty$, i.e.

$$\frac{3}{4}\pi + \phi_k \geq \phi_s \geq \frac{\pi}{4} + \phi_k, \quad \text{for } s \to 0$$

(5)

$$\frac{\pi}{4} > \phi_s > -\frac{\pi}{4}, \quad \text{for } s \to \infty.$$

(6)

which are satisfied by the path in Fig. 2. Integration of (4) along y' produces [10, p. 493]

$$\frac{1}{4j}H_0^{(2)}(kR) = \frac{1}{2\pi^{3/2}} \int_{-\infty}^\infty dy' \int_0^\infty e^{-[R^2+(y-y')^2]s^2+\frac{k^2}{4s^2}} ds.$$

(7)

In order to interchange the order of integration, we first note that convergence of the s-integral for $-\infty < y' < \infty$ is guaranteed by choosing the s-integration path such that $\text{Re}[(y - y')^2 s^2] > 0$, so that the constraint (6) and the complex path in Fig. 2 apply. Closed form integration in y' then leads to the Ewald transformation for 2-D cylindrical radiated fields

$$\frac{1}{4j}H_0^{(2)}(kR) = \frac{1}{2\pi} \int_0^\infty \frac{e^{-R^2s^2+\frac{k^2}{4s^2}}}{s} ds.$$

(8)

The Ewald method is obtained by splitting the integral in (8) into two parts, $\int_0^\infty = (\int_0^{\mathcal{E}} + \int_{\mathcal{E}}^\infty)$, which also determines the splitting $G = G_{\text{spectral}} + G_{\text{spatial}}$ of (1), shown in Section IV.

IV. GREEN'S FUNCTION TRANSFORMATION

Using (8) and the integral splitting above in (1) leads to the Green's function representation

$$G(\mathbf{r}, \mathbf{r}') = G_{\text{spectral}}(\mathbf{r}, \mathbf{r}') + G_{\text{spatial}}(\mathbf{r}, \mathbf{r}')$$

(9)

with

$$G_{\text{spectral}}(\mathbf{r}, \mathbf{r}') = \frac{1}{2\pi} \sum_{m=-\infty}^\infty e^{-jk_{x0}md}$$
$$\times \int_0^{\mathcal{E}} \frac{e^{-R_m^2 s^2+\frac{k^2}{4s^2}}}{s} ds$$

(10)

$$G_{\text{spatial}}(\mathbf{r}, \mathbf{r}') = \frac{1}{2\pi} \sum_{m=-\infty}^\infty e^{-jk_{x0}md}$$
$$\times \int_{\mathcal{E}}^\infty \frac{e^{-R_m^2 s^2+\frac{k^2}{4s^2}}}{s} ds$$

(11)

with complex paths of integration for G_{spectral} and G_{spatial} defined as the first and the second portions of the complex path shown in Fig. 2, respectively. The subscripts indicate that the corresponding Green's function contributions will be transformed to *modified* spectral and spatial representations, respectively. It is important to notice that the series G_{spectral} does not decay exponentially, while the series G_{spatial} has Gaussian convergence because $\text{Re}(s) > \mathcal{E}$ on the complex path of integration shown in Fig. 2. This can be simply seen in the following way. For large m, each m-integral in (11) becomes $\int_{\mathcal{E}}^\infty s^{-1}e^{-m^2 d^2 s^2} ds$. An integration by parts indicates that for large m, the terms in the series G_{spatial} asymptotically behave like $e^{-m^2 d^2 \mathcal{E}^2}/(m^2 d^2 \mathcal{E}^2)$ thus exhibiting Gaussian convergence. On the other hand, since the original m-terms of G (sum of the m-terms of G_{spectral} and G_{spatial}), decay like $1/\sqrt{m}$, the m- terms in G_{spectral} decay like $1/\sqrt{m}$. This latter convergence rate is accelerated in the following section.

A. Transformation of $G_{\text{spectral}}(\mathbf{r}, \mathbf{r}')$

Since the series in (10) does not decay exponentially, it is transformed using the Poisson summation formula [11, p. 117]

$$\sum_{m=-\infty}^\infty f(md) = \frac{1}{d} \sum_{p=-\infty}^\infty \tilde{f}\left(\frac{2\pi p}{d}\right)$$

(12)

$$\tilde{f}(k_x) = \int_{-\infty}^\infty f(\xi)e^{-jk_x\xi}d\xi$$

(13)

in which $\tilde{f}(2\pi p/d)$ is the spectrum of the function $f(x)$ sampled at $2\pi p/d$. We identify $f(md)$ with terms of (10)

$$f(md) = \frac{e^{-jk_{x0}md}}{2\pi}$$
$$\times \int_0^{\mathcal{E}} \frac{e^{-[(z-z')^2+(x-x'-md)^2]s^2+\frac{k^2}{4s^2}}}{s} ds \quad (14)$$

and thus

$$\tilde{f}\left(\frac{2\pi p}{d}\right) = \frac{1}{2\pi} \int_{-\infty}^{\infty} d\xi$$
$$\times \int_0^{\mathcal{E}} ds \frac{1}{s} e^{-[(z-z')^2+(x-x'-\xi)^2]s^2+\frac{k^2}{4s^2}} e^{-jk_{xp}\xi} \quad (15)$$

with

$$k_{xp} = k_{x0} + \frac{2\pi p}{d} \quad (16)$$

denoting the Floquet wavenumber along x. Before interchanging the order of integration, one must be sure that the s-integral is convergent along the path $(0, \mathcal{E})$ shown in Fig. 2 for $\xi \in (-\infty, \infty)$. Thus, analogous to the discussion preceding (8), we also require that $\text{Re}(s^2) > 0$, which is automatically satisfied with the chosen path in Fig. 2. Once this is ensured, interchange of the order of integration, followed by a closed form evaluation of the ξ-integral using the formula $\int_{-\infty}^{\infty} e^{-a\xi^2+b\xi} d\xi = \sqrt{\pi/a}\, e^{b^2/4a}$, leads to

$$\tilde{f}\left(\frac{2\pi p}{d}\right) = \frac{e^{-jk_{xp}(x-x')}}{2\sqrt{\pi}} \int_0^{\mathcal{E}} \frac{e^{-(z-z')^2 s^2} e^{k_{zp}^2/4s^2}}{s^2} ds \quad (17)$$

with

$$k_{zp} = \sqrt{k^2 - k_{xp}^2} \quad (18)$$

denoting the Floquet wavenumber along z. For convergence, we require $\text{Re}(k_{zp}^2/s^2) < 0$ on the path shown in Fig. 2. For evanescent Floquet waves (FWs), (p large) this is automatically satisfied since $\text{Re}(k_{zp}^2) < 0$. For propagating FWs (p small), convergence is ensured by the same argument preceding (6) since $\text{Re}(k_{zp}^2) > 0$ but $\text{Im}(k_{zp}^2) < 0$. The substitution $s' = 1/s$ results in

$$\tilde{f}\left(\frac{2\pi p}{d}\right) = \frac{e^{-jk_{xp}(x-x')}}{2\sqrt{\pi}} \int_{1/\mathcal{E}}^{\infty} e^{-(z-z')^2/s'^2} e^{\frac{k_{zp}^2 s'^2}{4}} ds' \quad (19)$$

and maps the domain of integration $(0, \mathcal{E})$ shown in Fig. 2, onto $(1/\mathcal{E}, \infty)$ with path constraints for $s' \to \infty$ imposed by those near $s = 0$. Therefore, $\text{Re}(k_{zp}^2 s'^2) < 0$ for every $p = 0, \pm 1, \pm 2, \ldots$. Expression (19) is now in a standard form (see [2] and [12, (7.4.33)]) to be transformed into

$$\tilde{f}\left(\frac{2\pi p}{d}\right) = \frac{e^{-jk_{xp}(x-x')}}{4jk_{zp}}$$
$$\times \left[e^{jk_{zp}|z-z'|} \text{erfc}\left(\frac{jk_{zp}}{2\mathcal{E}} + |z-z'|\mathcal{E}\right) \right.$$
$$\left. + e^{-jk_{zp}|z-z'|} \text{erfc}\left(\frac{jk_{zp}}{2\mathcal{E}} - |z-z'|\mathcal{E}\right) \right] (20)$$

obtained via the procedure of Appendix A. The transformed G_{spectral} in (10) is obtained by inserting (20) into (12), leading to

$$G_{\text{spectral}}(\mathbf{r},\mathbf{r}') = \frac{1}{4d} \sum_{p=-\infty}^{\infty} \frac{e^{-jk_{xp}(x-x')}}{jk_{zp}}$$
$$\times \left[e^{jk_{zp}|z-z'|} \text{erfc}\left(\frac{jk_{zp}}{2\mathcal{E}} + |z-z'|\mathcal{E}\right) \right.$$
$$\left. + e^{-jk_{zp}|z-z'|} \text{erfc}\left(\frac{jk_{zp}}{2\mathcal{E}} - |z-z'|\mathcal{E}\right) \right] (21)$$

in which $\text{erfc}(z)$ is the complementary error function

$$\text{erfc}(z) = \frac{2}{\sqrt{\pi}} \int_z^{\infty} e^{-t^2} dt. \quad (22)$$

B. Transformation of $G_{\text{spatial}}(\mathbf{r},\mathbf{r}')$

Efficient evaluation of the G_{spatial} series is based on evaluating the integral

$$I = \int_{\mathcal{E}}^{\infty} \frac{e^{-R_m^2 s^2 + \frac{k^2}{4s^2}}}{s} ds. \quad (23)$$

Following the procedure in [3], we first perform the change of variable $u = s^2$, then utilize the Taylor expansion $\exp[k^2/(4u)] = \sum_{q=0}^{\infty} (k/2)^{2q}/(q!\, u^q)$, and finally change to the variable $t = u/\mathcal{E}^2$. This leads to

$$I = \frac{1}{2} \sum_{q=0}^{\infty} \left(\frac{k}{2\mathcal{E}}\right)^{2q} \frac{1}{q!} E_{q+1}\left(R_m^2 \mathcal{E}^2\right) \quad (24)$$

in which $E_q(z)$ is the qth order exponential integral defined as [12, p. 228]

$$E_q(z) = \int_1^{\infty} \frac{e^{-zt}}{t^q} dt. \quad (25)$$

Insertion of (24) into (11) leads to the following representation of the modified spatial integral:

$$G_{\text{spatial}}(\mathbf{r},\mathbf{r}') = \frac{1}{4\pi} \sum_{m=-\infty}^{\infty} e^{-jk_{x0}md}$$
$$\times \sum_{q=0}^{\infty} \left(\frac{k}{2\mathcal{E}}\right)^{2q} \frac{1}{q!} E_{q+1}\left(R_m^2 \mathcal{E}^2\right). \quad (26)$$

From a numerical point of view, only the exponential integral $E_1(z)$ needs to be evaluated numerically using, for instance, the Algorithm A of [12, Sec. 5.1.53] for $0 \leq z \leq 1$, or [12, Sec. 5.1.56] for $1 \leq z < \infty$. Higher order exponential integrals may then be evaluated by the recurrence relation

$$E_{q+1}(z) = \frac{1}{q}[e^{-z} - zE_q(z)], \quad q = 1, 2, 3, \ldots. \quad (27)$$

V. DISCUSSION

A. Singular Contribution

When the distance between the observation point $\mathbf{r}$ and the source point $\mathbf{r}'$ or one of its periodic extensions is electrically

small, the contribution to the Green's function is essentially quasistatic. Singular terms in (1) or (26) often arise, for example, from one of the spatial terms R_m with $m = -1, m = 0$, or $m = +1$, depending on which term represents the source nearest to the observer $\mathbf{r}$. Assuming that $R_0 = |\mathbf{r} - \mathbf{r}'| \ll \lambda$ in (1), then $kR_0 \ll \pi$ and the $m = 0$ term of the element-by-element sum (1) provides the logarithmic singularity $1/(4j)H_0^{(2)}(kR_0) \approx -1/(2\pi)\ln(R_0)/(2\pi)$.

In the Ewald representation (9), the logarithmic singularity arises from the *spatial* series $G_{\text{spatial}}(\mathbf{r}, \mathbf{r}')$ in (26). Since $R_0 \ll \lambda$, the argument of the exponential integrals for the $m = 0$ term in (26) is $R_0^2\mathcal{E}^2 \ll \lambda^2\mathcal{E}^2$, which implies $R_0^2\mathcal{E}^2 \to 0$ when λ has the same order of magnitude of d and $\mathcal{E}$ is not too large (i.e., $\mathcal{E}$ given in Section V-C). According to [12, (5.1.12)], the small argument behavior of the exponential integrals is $E_{q+1}(z \approx 0) \approx -(-z)^q(\ln z)/q!$, and for $R_0 \to 0$, (26) behaves as

$$G(\mathbf{r}, \mathbf{r}') \approx G_{\text{spatial}}(\mathbf{r}, \mathbf{r}')$$
$$\approx \frac{1}{4\pi}\sum_{q=0}^{\infty}\left(\frac{k}{2\mathcal{E}}\right)^{2q}\frac{1}{q!}\left[-\frac{(-R_0^2\mathcal{E}^2)^q}{q!}\ln\left(R_0^2\mathcal{E}^2\right)\right]$$
$$\approx -\frac{1}{2\pi}\ln(R_0\mathcal{E}) \approx -\frac{1}{2\pi}\ln(R_0) \qquad (28)$$

in which only the $q = 0$ term has been retained since $R_0 \to 0$. Thus, (28) provides the same required logarithmic singularity for $R_0 \to 0$ as the element-by-element sum in (1).

B. Asymptotic Convergence of Series in G_{spectral} and G_{spatial}, and Optimum Splitting Parameter $\mathcal{E}_0$

We analyze here the convergence properties of G_{spectral} and G_{spatial} given by (21) and (26), respectively. In the *spectral* sum G_{spectral}, for large p, we can approximate $k_{xp} \approx 2\pi p/d$ and $k_{zp} \approx -j(2\pi p/d)$. Furthermore, the asymptotic expansion for the error function (22) for large argument, $\text{erfc}(z) \sim e^{-z^2}/(\sqrt{\pi}z)$, leads to the asymptotic behavior of terms with large p

$$\sim \frac{e^{-j2\pi p(x-x')/d}}{4\sqrt{\pi}d\mathcal{E}}\frac{e^{-\left(\frac{\pi p}{d\mathcal{E}}\right)^2}}{\left(\frac{\pi p}{d\mathcal{E}}\right)^2} \qquad (29)$$

which exhibits Gaussian p-convergence. In the *spatial* sum G_{spatial}, we can approximate $R_m \approx md$, and the large argument expansion for the exponential integral $E_{q+1}(z) \sim e^{-z}/z$ leads to the following asymptotic behavior of terms with large m:

$$\sim \frac{e^{\left(\frac{k}{2\mathcal{E}}\right)^2}}{4\pi}e^{-jk_{x0}md}\frac{e^{-(md\mathcal{E})^2}}{(md\mathcal{E})^2}. \qquad (30)$$

Thus, the series G_{spatial} also exhibits Gaussian m-convergence. The optimum $\mathcal{E}$ parameter, $\mathcal{E}_0$, minimizes the total number $M + P$ of necessary m, p-terms in (21) and (26). The total number of terms needed is determined by observing that to obtain roughly the same number of significant digits of accuracy in each sum in (21) and (26), we must set $(Md\mathcal{E})^2 = (P\pi)^2/(d\mathcal{E})^2 \equiv \sigma^2$. The minimum number of terms needed to achieve this accuracy

is thus $N^{\text{tot}} = \sigma[1/(d\mathcal{E}) + d\mathcal{E}/\pi]$. The optimum $\mathcal{E}_0$ parameter is obtained by imposing $\partial N^{\text{tot}}/\partial\mathcal{E} = 0$, which leads to

$$\mathcal{E}_0 = \frac{\sqrt{\pi}}{d}. \qquad (31)$$

It should be noted that the choice of the optimum splitting parameter $\mathcal{E} = \mathcal{E}_0$ results in both series, G_{spectral} in (21) and G_{spatial} in (26), converging asymptotically with identical Gaussian convergence rates, $\sim \exp(-\pi p^2)$ and $\sim \exp(-\pi m^2)$, respectively.

C. High-Frequency Breakdown of Ewald Representation

At high frequencies, some of the leading terms in the Ewald representation can become very large. In particular, exponentially large terms arise from the propagating terms (those with *real* k_{zp}), such as the $p = 0$ in the spectral sum G_{spectral} in (21). The two erfc functions in (21) provide (for example for $p = 0$) two terms that asymptotically behave like $\exp[k_{z0}^2/(4\mathcal{E}^2) - (z - z')^2\mathcal{E}^2]$ and which can cause a numerical instability when their argument is very large. This numerical instability arises from the Ewald splitting and is not physical. It is in fact compensated by other numerically large terms in the spatial sum G_{spatial} in (26), as can be easily seen from expression (11) where, when $k^2/(4\mathcal{E}^2) >> 1$, many m-terms can be very large until dominated by $-R_m^2\mathcal{E}^2$. Alternatively, this can be seen in (26) where it is noted that many p-terms are necessary to obtain convergence. Thus, at high frequencies, we have a loss of precision due to cancellation of large numbers when summing G_{spectral} and G_{spatial} in (9). This problem may be avoided by requiring that in the spectral sum $k_{z0}^2/(4\mathcal{E}^2) - (z - z')^2\mathcal{E}^2 < H^2$, where H^2 is the maximum exponent permitted, which leads to

$$\mathcal{E} > \mathcal{E}_1 \equiv \frac{H}{\sqrt{2}|z - z'|}$$
$$\times \left(\sqrt{1 + \frac{k_{z0}^2(z - z')^2}{H^4}} - 1\right)^{1/2} \approx \frac{k_{z0}}{2H}. \quad (32)$$

The last approximation is obtained assuming $k_{z0}|z - z'| \ll H^2$. For example, consider a worst case in which there is no phasing ($k_{x0} = 0$). If we require $H^2 = 9$ we need $\mathcal{E} > \mathcal{E}_1 \approx k/6 \approx 1/\lambda$. In other words, for $H^2 = 9$, the choice of the optimum parameter $\mathcal{E} = \mathcal{E}_0$ is a good choice if $d < 1.7\lambda$.

Even though the exponential growth is limited by the choice $\mathcal{E} > \mathcal{E}_1$, in order to have a computationally efficient algorithm we also require the q-sum in (26) to be rapidly convergent. From $(q - 1)q^{-1}E_q(x) < E_{q+1}(x) < E_q(x)$ [12, (5.1.17), p. 229] we infer that the exponential integral does not decay significantly with q, and indeed, except for $x \ll q$ and large q, $E_q(x) \approx e^{-x}/q$ ([12, (5.1.19), p. 229]). Thus, convergence of (26) relies on having $(k/2\mathcal{E})^{2q}/q!$ negligible for $q \geq Q$, i.e., $[k/(2\mathcal{E})]^{2Q}/Q! < \epsilon$, with ϵ the desired error and Q the number of q-terms necessary to achieve convergence (typically 10–15). This implies that

$$\mathcal{E} > \mathcal{E}_2 \equiv \frac{k}{2(\epsilon Q!)^{\frac{1}{2Q}}}. \qquad (33)$$

For example, if we require $\epsilon = 10^{-7}$, and $Q = 13$, we have $\mathcal{E} > \mathcal{E}_2 = k/2.56\,(\mathcal{E}_2 = 2.45/\lambda)$ that has to be considered jointly with (31).

Thus, for high frequencies, or equivalently for large interelement spacings $d > \lambda$, the constraints (33) and (32) force a choice of $\mathcal{E}$ other than "optimum" (31). We, therefore, suggest choosing

$$
\begin{aligned}
\mathcal{E} &= \max\{\mathcal{E}_0, \mathcal{E}_1, \mathcal{E}_2\} \\
&= \max\left\{\frac{\sqrt{\pi}}{d}, \frac{k_{z0}}{2H}, \frac{k}{2(\epsilon Q!)^{\frac{1}{2Q}}}\right\}
\end{aligned}
\tag{34}
$$

for the $\mathcal{E}$ parameter to be used in (21) and (26).

VI. GRADIENT OF THE PERIODIC GREEN'S FUNCTION

In many applications, not only the potential, but also the gradient of the periodic free space Green's function is required. The gradient of the periodic Green's function may be obtained simply by taking the gradient of the Ewald representation (9), yielding

$$
\nabla G(\mathbf{r}, \mathbf{r}') = \nabla G_{\text{spectral}}(\mathbf{r}, \mathbf{r}') + \nabla \mathbf{G}_{\text{spatial}}(\mathbf{r}, \mathbf{r}')
\tag{35}
$$

where

$$
\begin{aligned}
\nabla G_{\text{spectral}}(\mathbf{r}, \mathbf{r}') = \frac{1}{d} \sum_{p=-\infty}^{\infty} \frac{e^{-jk_{xp}(x-x')}}{4jk_{zp}} \\
\times \{[-j\hat{\boldsymbol{x}}k_{xp} - j\hat{\boldsymbol{z}}k_{zp}\text{sgn}(z-z')] \\
\times e^{-jk_{zp}|z-z'|}\text{erfc}\left(\frac{jk_{zp}}{2\mathcal{E}} - |z-z'|\mathcal{E}\right) \\
+ [-j\hat{\boldsymbol{x}}k_{xp} + j\hat{\boldsymbol{z}}k_{zp}\text{sgn}(z-z')] \\
\times e^{jk_{zp}|z-z'|}\text{erfc}\left(\frac{jk_{zp}}{2\mathcal{E}} + |z-z'|\mathcal{E}\right) \\
- \hat{\boldsymbol{z}}\,\text{sgn}(z-z')\mathcal{E}e^{-jk_{zp}|z-z'|} \\
\times \text{erfc}'\left(\frac{jk_{zp}}{2\mathcal{E}} - |z-z'|\mathcal{E}\right) \\
+ \hat{\boldsymbol{z}}\,\text{sgn}(z-z')\mathcal{E}e^{jk_{zp}|z-z'|} \\
\times \text{erfc}'\left(\frac{jk_{zp}}{2\mathcal{E}} + |z-z'|\mathcal{E}\right)\}
\end{aligned}
\tag{36}
$$

with (a prime denotes differentiation)

$$
\text{erfc}'(z) = -\frac{2}{\sqrt{\pi}}e^{-z^2}
$$

and

$$
\begin{aligned}
\nabla G_{\text{spatial}}(\mathbf{r}, \mathbf{r}') = \frac{-\mathcal{E}^2}{2\pi} \sum_{m=-\infty}^{\infty} [\hat{\boldsymbol{x}}(x - x' - md) \\
+ \hat{\boldsymbol{z}}(z - z')]e^{-jk_{x0}md} \\
\times \sum_{q=0}^{\infty}\left(\frac{k}{2\mathcal{E}}\right)^{2q}\frac{1}{q!}E_q\left(R_m^2\mathcal{E}^2\right)
\end{aligned}
\tag{37}
$$

in which we have used the property $E'_{q+1}(z) = -E_q(z)$, with the definition $E_0(z) \equiv e^{-z}/z$. The vectors $\hat{\boldsymbol{x}}$ and $\hat{\boldsymbol{z}}$ denote unit vectors along the x and z coordinates, respectively. The two series $\nabla G_{\text{spectral}}$ and $\nabla G_{\text{spatial}}$ exhibit Gaussian convergence.

A. Singular Contribution

When the argument $R_m^2\mathcal{E}^2$ is small—which without loss of generality we assume occurs for the $m = 0$ term—the gradient of the element-by-element sum representation of the Green's function, (1), is dominated by the $m = 0$ term, i.e., $\nabla G \approx -k[\hat{\boldsymbol{x}}(x - x') + \hat{\boldsymbol{z}}(z - z')]H_1^{(2)}(kR_0)/(4jR_0)$. For small argument x, $H_1^{(2)}(x) \approx j2/(\pi x) - j(x/\pi)\ln(x/2) + (x/2)[1 + j(1 - 2\gamma)/\pi]$, with $\gamma = 0.577\,215\,66$ the Euler constant, has a dominant pole singularity. In the Ewald representation (35), it is the spatial sum $\nabla G_{\text{spatial}}(\mathbf{r}, \mathbf{r}')$ that exhibits the pole singularity due to the $E_q(R_m^2\mathcal{E}^2)$ terms in (37). Indeed, for $R_0 \to 0$, the $m = 0, q = 0$ term in $\nabla G_{\text{spatial}}(\mathbf{r}, \mathbf{r}')$ dominates and

$$
\begin{aligned}
\nabla G(\mathbf{r}, \mathbf{r}') &\approx \nabla G_{\text{spatial}}(\mathbf{r}, \mathbf{r}') \\
&\approx -\frac{[\hat{\boldsymbol{x}}(x - x') + \hat{\boldsymbol{z}}(z - z')]}{2\pi R_0^2}
\end{aligned}
\tag{38}
$$

which has the same pole singularity of the gradient as the element-by-element sum (1).

VII. NUMERICAL EXAMPLE: CONVERGENCE

We analyze in Fig. 3 the convergence rate of the Ewald sums using the percent relative error defined as $\text{Err} = |G^{\text{exact}} - G^{\text{Ewald}}|/|G^{\text{exact}}| \times 100$, where G^{exact} is the Green's function reference solution (1) evaluated via its spectral counterpart with sufficiently large number of terms to achieve accuracy up to seven decimal digits, and G^{Ewald} is the same Green's function evaluated using the Ewald splitting (9) with (21) and (26). The percentage relative error is plotted versus summation limit parameters $\pm M, \pm P$ in sums (21) and (26) resulting in a total number of terms of $2M + 1$ and $2P + 1$, respectively. For simplicity the array is nonphased, i.e., $k_{x0} = 0$. The $m = 0$ line source is at $(x', z') = (0, 0)$, and the two curves are related to two observation points at $(x, z) = (d/2, 0)$ and $(x, z) = (d/2, d/2)$, respectively.

In Fig. 3(a) the error is plotted versus M, with $P = M$, for an array of line sources with spacings $d = 0.06\lambda$, where $\lambda = 2\pi/k$ is the free space wavelength. In accordance with (34), the Ewald splitting parameter $\mathcal{E}$ is chosen as its optimum value, $\mathcal{E}_0$. Indeed, in (21), (26), $k/(2\mathcal{E}) = k_{z0}/(2\mathcal{E}) = 0.1063$ (we recall that $k_{x0} = 0$) is a small number that does not cause a numerical loss of precision for the reasons outlined in Section V-C. A large total number $Q = 40$ of terms in (26) has been used because we emphasize here convergence issues related only to $\mathcal{E}, M$, and P.

In Fig. 3(b), the frequency is increased such that $d = 0.6\lambda$. Again, in accord with (34), we choose the optimum parameter, i.e., $\mathcal{E} = \mathcal{E}_0$. In this case $k/(2\mathcal{E}) = k_{z0}/(2\mathcal{E}) = 1.063$ is still not large enough to cause numerical errors in (21) and (26).

In Fig. 3(c), the frequency is further increased such that $d = 6.5\lambda$ and the high frequency breakdown problem described in Section V-C occurs. In this case we cannot choose the optimum parameter $\mathcal{E} = \mathcal{E}_0$. Indeed, if we did, we would have $k_{z0}/(2\mathcal{E}) = 11.52$ in (21), yielding terms on the order of e^{133} that would cause overflow or at least loss of accuracy. Furthermore, in (26) we would have $k/(2\mathcal{E}) = 11.52$, thus requiring a very large number of q-terms to achieve convergence in addition to the loss of accuracy due to large values
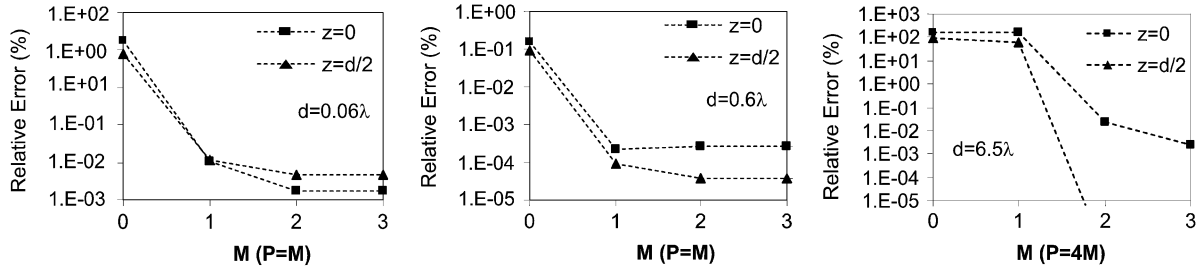
Fig. 3.   Convergence of the Ewald sums in (9) with (21) and (26). Percentage relative error versus number of terms M [$P = M$ in (a) and (b), and $P = 4M$ in (c)] in sums (21) and (26). Three different frequencies are considered such that (a) $d = 0.06\lambda$, (b) $d = 0.6\lambda$, and (c) $d = 6.5\lambda$.

involved in that sum. The Ewald splitting parameter $\mathcal{E}$ must therefore be chosen according to (34). The rate of convergence of the two series in (21), (26) is then different, and more terms ($P > M$) in G_{spectral} (21) are needed in order to maintain the same relative error in both (21) and (26).

Note that a *very* small number of terms in G_{spectral} and G_{spatial} is required to achieve a percentage error smaller then 0.001%. In our cases the relative error cannot be further decreased by augmenting the number of terms P, M in $G_{\text{spectral}}, G_{\text{spatial}}$ because of accuracy limits of the numerical subroutines that evaluate the error functions in G_{spectral} and the exponential integral $E_1(z)$ in G_{spatial} (see [13] for $\text{erfc}(z)$, and [12, Sec. 5.1.53, 5.1.56] for $E_1(z)$).

Figs. 4 and 5 show the rate of convergence of the two individual series G_{spectral} and G_{spatial} in (21) and (26), respectively, evaluated at the location $(x, z) = (d/2, 0)$. The relative error is defined as

$$\text{Err}_{\text{spectral,spatial}} = \frac{|G_{\text{spectral,spatial}}^{\text{Ewald,exact}} - G_{\text{spectral,spatial}}^{\text{Ewald},P,M}|}{|G_{\text{spectral,spatial}}^{\text{Ewald,exact}}|} \times 100 \tag{39}$$

where $G_{\text{spectral,spatial}}^{\text{Ewald,exact}}$ is either G_{spectral} or G_{spatial} evaluated with a sufficient number of terms to achieve high numerical accuracy. The error is plotted versus the summation limit parameters $\pm P$ and $\pm M$ employed in the sums in G_{spectral} and in G_{spatial}, respectively (in particular, $-P \leq p \leq P$, and $-M \leq m \leq M$).

In Fig. 4, the array is the same as that in Fig. 3(b), i.e., $d = 0.6\lambda$, and the two series need the *same* number of terms to achieve the same accuracy since we have chosen $\mathcal{E} = \mathcal{E}_0$. It is remarkable that only a few terms are required to achieve high accuracy.

In Fig. 5, the array is the same as that in Fig. 3(c), i.e., $d = 6.5\lambda$, and the two series in G_{spectral} and G_{spatial} need *different* numbers of terms to achieve the same accuracy since we have chosen $\mathcal{E} = \mathcal{E}_1 > \mathcal{E}_0$. In particular in Fig. 5(a) we have set $H = 3.5$ [see (34)], implying that $\mathcal{E}_1/\mathcal{E}_0 = 3.29$, and it is clearly seen that a larger number of terms in G_{spectral} is required. In Fig. 5(b) we have set $H = 3$ (i.e., $\mathcal{E}_1/\mathcal{E}_0 = 3.84$) and in G_{spectral} a larger number of terms is required with respect to the previous case. Fig. 5(c) shows the need for an even larger number of terms for $H = 2.5 (\mathcal{E}_1/\mathcal{E}_0 = 4.61)$.

Clearly, choosing a larger H (i.e., smaller $\mathcal{E}_1/\mathcal{E}_0$) bounds the growth of the number of terms in G_{spectral}. Unfortunately, H cannot be chosen too large because, as explained in Section V-C, it would generate values on the order of e^{H^2}. It should also be
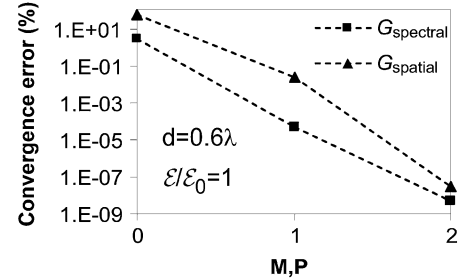

Fig. 4.   Convergence rates for series G_{spectral} and G_{spatial}, in (21) and (26), respectively. Here, $d = 0.6\lambda$ as in Fig. 3(b). For the choice of the optimum parameter $\mathcal{E} = \mathcal{E}_0$, the two series G_{spectral} and G_{spatial} have the same convergence rate, as explained in Section V-B.

noted that choosing $\mathcal{E} = \mathcal{E}_1$, with decreasing $H = 3.5, 3, 2.5$, automatically implies that the values in the series G_{spatial} become smaller and smaller compared to those in G_{spectral}. For an array with $d = 6.5\lambda$, values of $H > 3.5$ (i.e., $\mathcal{E}_1/\mathcal{E}_0 < 3.29$) would already cause a small loss of accuracy, while $H < 2.5$ (i.e., $\mathcal{E}_1/\mathcal{E}_0 > 4.61$) would require too many terms in the G_{spectral} sum.

VIII. CONCLUSION

The Green's function for a periodic array of phased line sources has been efficiently represented using the Ewald representation for cylindrical waves. The array is assumed to be of infinite extent, so this method applies to finite structures as a first approximation. For a correct treatment of finite periodic structures some modifications would be required. The resulting series have Gaussian convergence and only a few terms are needed to achieve good accuracy. Also, the influence of the Ewald splitting parameter and frequency on the convergence properties of the series has been analyzed analytically and numerically. We have proposed an automatic choice of the Ewald parameter that depends on the ratio between the array period and the free space wavelength for high frequencies. Preliminary results for the Green's function representation for 1-D periodic multilayered media (a 2-D problem) using the Ewald scheme have been presented in [14], using the methodology in [4] for the 3-D case, and will be detailed in a future publication. The rapidly convergent Ewald representation has been used with the method of moments to accelerate the fill time of impedance matrices, leading to efficient numerical codes for analyzing gratings and 1-D periodic arrays. Compared to the standard plane wave representation of the Green's function, the use of the Ewald representation results in a large reduction of the fill time of the MoM matrix. This advantages have been observed
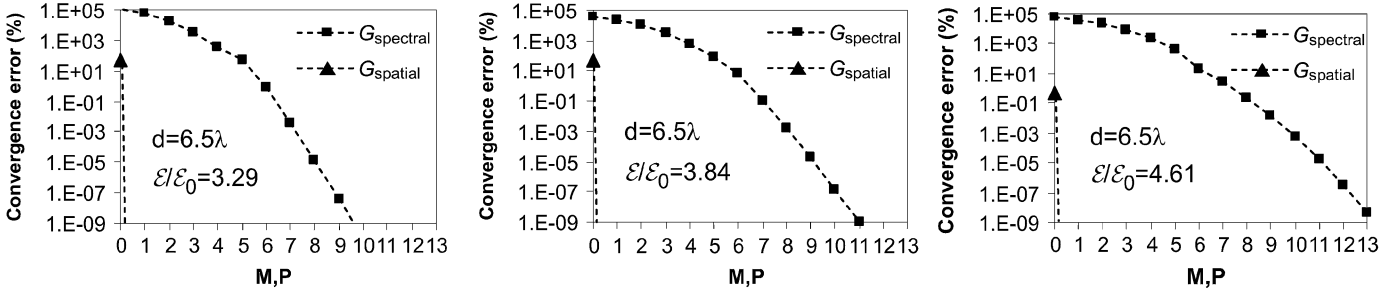
Fig. 5. Convergence rates for series G_{spectral} and G_{spatial}, in (21) and (26), respectively. Here, $d = 6.5\lambda$ as in Fig. 3(c). In this case the choice of the optimum parameter $E = E_0$ would cause numerical errors, as explained in Section V-B. Three different choices of the E parameters are here analyzed. Increasing the ratio E/E_0 results in a larger number of terms in G_{spectral} to reach convergence. A smaller ratio E/E_0 would decrease the number of necessary terms in G_{spectral} but it would cause loss of accuracy.

in [14] where we analyzed a periodic set of metallic enclosures in a multilayered environment. Furthermore, we have applied the Ewald acceleration in [15] to build a physically-based MOM preconditioner for the analysis of truncated arrays of 2-D metallic objects. The Ewald acceleration was necessary to have a reasonable computation time of the preconditioner, that otherwise would have been too computationally expensive when using a standard plane wave superposition. Recently, the Ewald algorithm has been applied in [16] to find the field radiated by a single line source located above a periodic EBG (electromagnetic band-gap) material or a periodic corrugated surface, and in [17] for studying the excitation of a 2-D EBG waveguide excited by a line source. Also, in this case the use of the standard plane wave superposition would have resulted in an much slower algorithm.

A formulation analogous to the present one has also been successfully applied to accelerate the Green's function for a periodic linear array of point sources (1-D periodicity) and will be reported in the future.

APPENDIX
DETAILS LEADING TO (20)

The integral (19) is evaluated here by performing the change of variable $u = |z - z'|/s' + jk_{zp}s'/2$, with $s' = (jk_{zp})^{-1}[u + (u^2 - 2jk_{zp}|z - z'|)]$, which transforms (19) into

$$\tilde{f}\left(\frac{2\pi p}{d}\right)$$
$$= \frac{e^{-jk_{xp}(x-x')}}{2\sqrt{\pi}} \frac{e^{jk_{zp}|z-z'|}}{jk_{zp}}$$
$$\times \int_{|z-z'|\mathcal{E}+\frac{jk_{zp}}{2\mathcal{E}}}^{\infty} e^{-u^2}\left(1 + \frac{u}{\sqrt{u^2 - j2k_{zp}|z-z'|}}\right) du. \tag{40}$$

Recalling the definition of the complementary error function (22), this yields

$$\tilde{f}\left(\frac{2\pi p}{d}\right) = \frac{e^{-jk_{xp}(x-x')}}{4}$$
$$\times \left[\frac{e^{jk_{zp}|z-z'|}}{jk_{zp}}\text{erfc}\left(|z-z'|\mathcal{E} + \frac{jk_{zp}}{2\mathcal{E}}\right) + I'\right] \tag{41}$$

in which I' is the remaining integral

$$I' = \frac{e^{jk_{zp}|z-z'|}}{jk_{zp}}\frac{2}{\sqrt{\pi}}$$
$$\times \int_{|z-z'|\mathcal{E}+\frac{jk_{zp}}{2\mathcal{E}}}^{\infty} e^{-u^2}\left(\frac{u}{\sqrt{u^2 - j2k_{zp}|z-z'|}}\right) du. \tag{42}$$

The change of variable $w = \sqrt{u^2 - 2jk_{zp}|z-z'|}$, together with (22), transforms I' into

$$I' = \frac{e^{-jk_{zp}|z-z'|}}{jk_{zp}}\text{erfc}\left(|z-z'|\mathcal{E} - \frac{jk_{zp}}{2\mathcal{E}}\right) \tag{43}$$

which is inserted into (41), providing (20).

REFERENCES

[1] P. P. Ewald, "Die berechnung optischer und elektrostatischen gitterpotentiale," *Ann. der Physik*, vol. 64, pp. 253–287, 1921. Translated by A. Cornell, Atomics International Libray, 1964.
[2] K. E. Jordan, G. R. Richter, and P. Sheng, "An efficient numerical evaluation of the Green's function for the Helmholtz operator on periodic structures," *J. Comp. Phys.*, vol. 63, pp. 222–235, 1986.
[3] A. W. Mathis and A. F. Peterson, "A comparison of acceleration procedures for the two-dimensinal periodic Green's function," *IEEE Trans. Antennas Propag.*, vol. 44, no. 4, pp. 567–571, Apr. 1996.
[4] D. R. Jackson, D. R. Wilton, and N. J. Champagne, "Efficient computation of periodic and nonperiodic Green's function in layered media using the MPIE," presented at the URSI Int. Symp. Electrom. Theory, Thessaloniki, Greece, May 25–28, 1998.
[5] M.-J. Park and S. Nam, "Efficient calculation of the Green's function for multilaayered planar periodic structures," *IEEE Trans. Antennas Propag.*, vol. 46, no. 10, pp. 1582–1583, Oct. 1998.
[6] M.-J. Park, J. Park, and S. Nam, "Efficient calculation of the Green's function for the rectangular cavity," *IEEE Trans. Microw. Guided Wave Lett.*, vol. 8, no. 3, pp. 124–126, Mar. 1998.
[7] C. M. Linton, "The Green's function for the two-dimensional Helmoltz equation in periodic domains," *J. Eng. Math.*, vol. 33, pp. 377–402, 1998.
[8] A. Kustepely and A. Q. Martin, "On the splitting parameter in the Ewald method," *IEEE Trans. Microw. Guided Wave Lett.*, vol. 10, no. 5, pp. 168–170, May 2000.
[9] E. Cohen, "Critical distance for grating lobe series," *IEEE Trans. Antennas Propag.*, vol. 39, no. 5, pp. 677–679, May 1991.
[10] L. B. Felsen and N. Marcuvitz, *Radiation and Scattering of Waves*. Englewood Cliffs, NJ: Prentice-Hall, 1973.
[11] A. Papoulis, *Systems and Transforms with Application in Optics*. Malabar, FL: R.E. Krieger, 1981.
[12] M. Abramowitz and I. A. Stegun, *Handbook of Mathematical Functions*. New York: Dover, 1970.
[13] J. A. C. Weideman, "Computation of the complex error function," *SIAM J. Numer. Anal.*, vol. 31, no. 5, pp. 1497–1518, 1994.
[14] F. Capolino, D. R. Wilton, and W. A. Johnson, "Efficient computation of the 2-D Green's function for 1-D periodic layered structures using the Ewald method," presented at the IEEE AP-S Symp., San Antonio, TX, Jun. 16–21, 2002.

[15] F. Capolino, D. R. Wilton, and D. R. Jackson, "Physical preconditioning for modeling 2-D large periodic arrays," presented at the IEEE AP-S Symp., San Antonio, TX, Jun. 16–21, 2002.

[16] F. Capolino, D. R. Jackson, and D. R. Wilton, "Fundamental properties of the field at the interface between air and a periodic artificial material excited by a line source," *IEEE Trans. Antennas Propag.*, vol. 53, no. 1, pp. 91–99, Jan. 2005.

[17] F. Capolino, D. R. Jackson, and D. R. Wilton, "Mode excitation from sources in two-dimensional EBG waveguides using the array scanning method," *IEEE Microw. Wireless Compon. Lett.*, vol. 15, no. 2, pp. 49–51, Feb. 2005.

Filippo Capolino (S'94–M'97–SM'04) was born in Florence, Italy, in 1967. He received the Laurea degree (*cum laude*) in electronic engineering and the Ph.D. degree from the University of Florence, Florence, Italy, in 1993 and 1997, respectively.

From 1994 to 2000, he was a Lecturer of antennas at the Diploma di Laurea, University of Siena, Italy, where he has been a Research Associate until 2002 and presently employed as an Assistant Professor. From 1997 to 1998, he was a Fulbright Research Visitor with the Department of Aerospace and Mechanical Engineering, Boston University, Boston, MA, where he continued his research with a Grant from the Italian National Council for Research (CNR), from 1998 to 1999. From 2000 to 2001, he was Research Assistant Visiting Professor with the Department of Electrical and Computer Engineering, University of Houston, Houston, TX, where he is now an Adjunct Assistant Professor. In November to December 2003, he was an Invited Assistant Professor at the Institut Fresnel, Marseille, France. His primary research interests are in high-frequency, short-pulse radiation, array antennas, periodic structures, and metamaterials. He is the coordinator of the Siena Unit for the Network of Excellence "Metamorphose" on Metamaterials of the EU FP6.

Dr. Capolino was awarded with a MMET'94 Student Paper Competition Award in 1994, the Raj Mittra Travel Grant for Young Scientists in 1996, the "Barzilai" prize for the best paper at the National Italian Congress of Electromagnetism (XI RiNEm) in 1996, and a Young Scientist Award for participating at the URSI International Symposium on Electromagnetics. Theory in 1998. He received the R. W. P. King Prize Paper Award from the IEEE Antennas and Propagation Society for the Best Paper of the Year 2000, by an author under 36. He is an Associate Editor for the IEEE TRANSACTIONS OF ANTENNAS AND PROPAGATION.

Donald R. Wilton (S'63–M'65–SM'80–F'87) was born in Lawton, OK, October 25, 1942. He received the B.S., M.S., and Ph.D. degrees from the University of Illinois, Urbana-Champaign, in 1964, 1966, and 1970, respectively.

From 1965 to 1968, he was with Hughes Aircraft Company, Fullerton, CA, engaged in the analysis and design of phased array antennas. From 1970 to 1983, he was with the Department of Electrical Engineering, University of Mississippi, University, and since 1983, he has been Professor of Electrical Engineering at the University of Houston, Houston, TX. From 1978 to 1979, he was a Visiting Professor at Syracuse University, Syracuse, NY. His primary research interest is in computational electromagnetics, and he has published, lectured, and consulted extensively in this area.

Dr. Wilton is a Member of Commission B of the International Union of Radio Science (URSI). He received the IEEE Third Millennium Medal and the Distinguished Alumni Award from the ECE Department, University of Illinois. He has served as Secretary (two terms), Technical Activities Committee Chair, Vice Chair, and Chair of U.S. Commission B of the URSI, and was also Member-at-Large of USNC/URSI. He has served the IEEE Antennas and Propagation Society as an Associate Editor of the IEEE TRANSACTIONS ON ANTENNAS AND PROPAGATION, as a Distinguished National Lecturer, and as a member of AdCom. He is an Associate Editor of the IEEE Press *Series on Electromagnetics*.

William A. Johnson (M'00–SM'02) was born in Beverly, MA, on April 26, 1951. He received the B.S., M.A., and Ph.D. degrees in mathematics, with minors in physics, from the University of Arizona, Tucson, in 1972, 1974, and 1978, respectively.

From 1978 to 1979, he was an Assistant Professor with the University of Mississippi, University. From 1979 to 1981, he was with Science Applications, Incorporated. From 1981 to 1983, he was with Lawrence Livermore National Laboratories, Livermore, CA, operated by the University of California for the U.S. Department of Energy. Since 1983, he has been with Sandia National Laboratories, Albuquerque, NM, where he is currently a Distinguished Member of the Technical Staff. He is also an adjunct Associate Professor for the Department of Mathematics at the University of New Mexico, Albuquerque.

Dr. Johnson is a Member of Commission B of the International Union of Radio Science (URSI).